# Title: Controlling Action Potentials With Magnetoelectric Nanoparticles

**Authors**: Elric Zhang<sup>1</sup>, Max Shotbolt<sup>2</sup>, Chen-Yu Chang<sup>3</sup>, Aidan Scott-Vandeusen<sup>2</sup>, Shawnus Chen<sup>4</sup>, Ping Liang<sup>5</sup>, Daniela Radu<sup>3</sup>, Sakhrat Khizroev<sup>1,6\*</sup>

#### **Affiliations**:

5

10

<sup>1</sup>Department of Electrical and Computer Engineering, University of Miami, Coral Gables, FL, USA.

<sup>2</sup>Department of Biomedical Engineering, University of Miami, Coral Gables, FL, USA.

<sup>3</sup>Department of Mechanical and Materials Engineering, Florida International University, Miami, FL, USA

<sup>4</sup>Department of Chemical, Environmental and Materials Engineering, Coral Gables, FL, University of Miami, USA.

<sup>5</sup>Cellular Nanomed, Irvine, CA, USA

<sup>6</sup>The Miami Project to Cure Paralysis, Department of Biochemistry and Molecular Biology, Miller School of Medicine, University of Miami, Miami, FL, USA.

\*Corresponding author. E-mail: <a href="mailto:skhizroev@miami.edu">skhizroev@miami.edu</a>

#### **Abstract:**

5

10

15

20

25

30

35

Non-invasive or minutely invasive and wireless brain stimulation that can target any region of the brain is an open problem in engineering and neuroscience with serious implications for the treatment of numerous neurological diseases. Despite significant recent progress in advancing new methods of neuromodulation, none has successfully replicated the efficacy of traditional wired stimulation and improved on its downsides without introducing new complications. Due to the capability to convert magnetic fields into local electric fields, MagnetoElectric NanoParticle (MENP) neuromodulation is a recently proposed framework based on new materials that can locally sensitize neurons to specific, low-strength alternating current (AC) magnetic fields (50Hz 1.7kOe field). However, the current research into this neuromodulation concept is at a very early stage, and the theoretically feasible game-changing advantages remain to be proven experimentally. To break this stalemate phase, this study leveraged understanding of the nonlinear properties of MENPs and the nanoparticles' field interaction with the cellular microenvironment. Particularly, the applied magnetic field's strength and frequency were tailored to the M-H hysteresis loop of the nanoparticles. Furthermore, rectangular prisms instead of the more traditional "spherical" nanoparticle shapes were used to: (i) maximize the magnetoelectric effect and (ii) improve the nanoparticle-cell-membrane surface interface. Neuromodulation performance was evaluated in a series of exploratory in vitro experiments on 2446 rat hippocampus neurons. Linear mixed effect models were used to ensure the independence of samples by accounting for fixed adjacency effects in synchronized firing. Neural activity was measured over repeated 4-minute segments, containing 90 seconds of baseline measurements, 90 seconds of stimulation measurements, and 60 seconds of post stimulation measurements. 87.5% of stimulation attempts produced statistically significant (P < 0.05) changes in neural activity, with 58.3% producing large changes (P < 0.01). In negative controls using either zero or 1.7kOe-strength field without nanoparticles, no experiments produced significant changes in neural activity (P > 0.05 and P > 0.15 respectively). Furthermore, an exploratory analysis of a direct current (DC) magnetic field indicated that the DC field could be used with MENPs to inhibit neuron activity (P < 0.01). These experiments demonstrated the potential for magnetoelectric neuromodulation to offer a near one-to-one functionality match with conventional electrode stimulation without requiring surgical intervention or genetic modification to achieve success, instead relying on physical properties of these nanoparticles as "On/Off" control mechanisms.

#### **One-Sentence Summary:**

This in vitro neural cell culture study explores how to exploit the non-linear and anisotropic properties of magnetoelectric nanoparticles for wireless neuromodulation, the importance of magnetic field strength and frequency matching for optimization, and demonstrates, for the first time, that magnetoelectric neuromodulation can inhibit neural responses.

#### INTRODUCTION

5

10

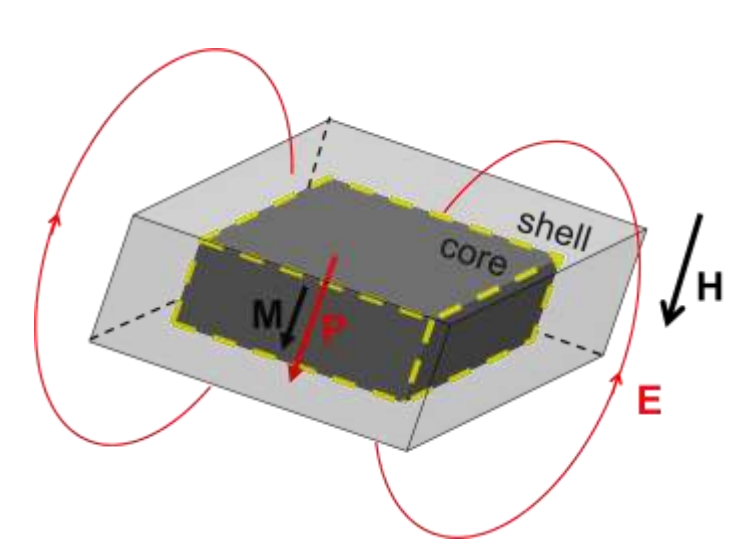
15

20

25

Electric fields are central to many critical biological functions. For some time now, we've known that carefully applied electric fields can significantly modify neural functions. The classical approach to applying electric fields within the brain relies on implantable electrodes or electrode arrays, which benefits from high temporal (ms) and spatial precision (< mm), ability to record inputs as well as stimulate, and low overall power requirements. This approach is already in use to diagnose and treat numerous neurodegenerative diseases and psychiatric disorders<sup>1</sup>. However, this approach is not without limitations. Implanting wires is an inherently invasive process, carrying risks of infection<sup>2,3</sup>, possibly requiring hardware reinsertion, and facing long term efficacy concerns from inflammatory responses<sup>4,5</sup>. These risks mean that electrode methods are typically last resort options for patients who do not respond to other, drug-based treatments. Furthermore, these methods are constrained mostly to treatment requirements, as it remains too risky to use as an exploratory tool in humans. As such, the fundamental mechanism behind the treatment modalities remains largely unknown<sup>6</sup>. These limitations have opened the question of whether there can be a better approach that achieves the same clinical effectiveness while improving on the invasive nature, which are commonly referred to as minimally invasive or non-invasive neuromodulation strategies<sup>7</sup>. In the last few decades, several prospective strategies have emerged, ranging from the fully wireless delivery of electric fields in Transcranial Magnetic Stimulation (TMS) and transcranial Alternating or Direct Current Stimulation (tACS, tDCS)<sup>7-11</sup>, to the use of intermediary changes in membranes in Optogenetics<sup>12</sup> and focused ultrasound (FUS)<sup>13–15</sup>. These methods have near universally offered some level of neuromodulation while reducing or eliminating the surgical requirements, but they have also introduced new challenges. Fully wireless methods such as TMS and TCS are truly non-invasive, but their mechanism of delivering energy through the volume of brain matter has thus far limited their usefulness to near-surface cortical

stimulation (~2cm). New approaches based on interference-based techniques have improved how deeply they can safely target<sup>16</sup>, but their spatial resolution remains relatively poor compared to electrodes, limited to spot sizes of several centimeters. Optogenetics has offered unrivaled spatial resolution (<1mm) and comparable temporal resolution (ms), but the necessity of extensive genetic modification with limited long-term studies and some continued reliance on surgical intervention complicates the clinical picture in humans. FUS has shown repeated success in stimulating even relatively deep regions in the brain across multiple studies<sup>15,17,18</sup>, but signal attenuation through the skull creates large variations in delivered power<sup>19</sup>, and treatment modalities are more focused on higher risk, ablative approaches that are currently less successful than DBS treatments<sup>20</sup>.



5

10

15

20

Figure 1: Core-shell MENP and Coupled Magnetic and Electric Fields. Core and shell are lattice-matched at their surface interface, thus enabling strain propagation between the magnetostrictive core and the piezoelectric shell, in turn coupling magnetic and electric fields. M is the core's magnetization, P is the shell's polarization, H is the magnetic field, E is the electric field. The illustrated relatively flat rectangular prism shape is intentional to promote anisotropy favorable for the MENP's coupling to the membrane surface.

A few groups, including ours, have turned to nanoparticle mediated approaches based on magnetothermal<sup>21,22</sup>, magnetomechanical<sup>23</sup>, and magnetoelectric stimulation<sup>24–28</sup> as an alternative.

Nanoparticle mediation has a few advantages. As the nanoparticles can act as transducers, it's possible to use otherwise sub-threshold or non-interacting fields and convert them into the relevant energies locally in the brain. Furthermore, nanoparticles below a critical size or with the help of specific coatings can cross the blood-brain barrier (BBB)<sup>29–31</sup>, providing a pathway to non-surgical delivery. In the case of Magnetoelectric nanoparticles (MENPs), they convert low power (10-150 mT) and low frequency (1-1000Hz) magnetic fields into hyper local electric fields, which then directly modulate neuron behavior. The use of electric fields gives MENPs a temporal advantage over other nanoparticle methods, which rely on secondary mechanisms with slower response times (>1s).

5

10

15

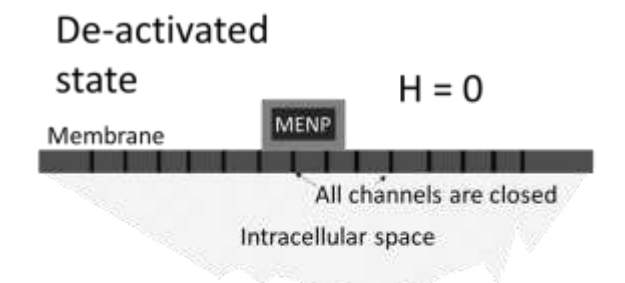
20

The premise of wireless magnetoelectric neuromodulation has already been demonstrated in *in vitro* <sup>26</sup>, *ex vivo* <sup>27</sup>, and *in vivo* <sup>28</sup> experiments, as well as in related problems of neuron stem cell differentiation <sup>32</sup> and directed neuron growth <sup>33</sup>. Furthermore, they can cross the blood-brain barrier <sup>34–36</sup> and have controllable clearance rates <sup>35</sup>. Additionally, several studies have demonstrated the biocompatibility of MENPs <sup>34,37–39</sup> To date, most medical application studies have used core-shell nanoparticles made of magnetostrictive and piezoelectric materials (**Fig. 1**) <sup>40</sup>. The origin of the ME effect in this two-phase nanostructure is due to strain propagation at the lattice-matched surface interface between the two phases. In a trivial linear approximation, the underlying physics of the ME effect in the core-shell MENPs can be described by the phenomenological Landau-Ginzburg-Devonshire (LLD) equation, originally derived for (single-phase) multiferroics <sup>41</sup>:

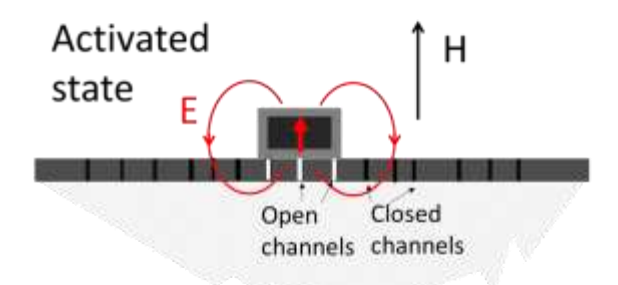
$$P_i = \alpha_i H_i, \tag{1}$$

where  $P_i$  and  $H_i$  stand for the i-th components of the polarization and the applied magnetic field, respectively,  $\alpha_i$  is the i-th diagonal term of the magnetoelectric coefficient tensor, assuming zero

cross-field terms. In turn, the induced local dipolar electric fields enable wirelessly controlled electric field modulation of neural activity <sup>26–28,42</sup>. The underlying mechanism of the MENPs-based approach is illustrated in **Fig. 2**. Because this approach can use relatively slow and low magnetic fields to transfer energy, its spatiotemporal resolution is not limited by interference with either skull or tissue media, and it doesn't induce destructive eddy currents. Furthermore, it works without relying on genetic modification for neural activation. Therefore, in theory, MENPs neuromodulation has the potential to overcome the aforementioned open problems of wireless high-resolution deep brain stimulation<sup>43</sup>.



5



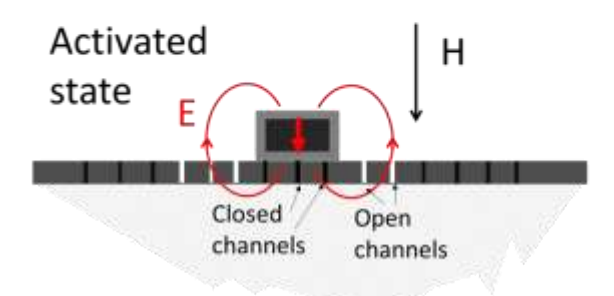


**Figure 2: Underlying Mechanism**: MENP placed on the membrane becomes an integral part of the membrane, which in turn allows to wirelessly control local voltage-controlled ion channels via

application of magnetic fields, thus controlling neural activation. (Top) With no magnetic field applied, the nanoparticle is depolarized/demagnetized, thus not affecting the membrane ion channels. (Middle and Bottom) Magnetic fields applied in opposite orientations open and close certain ion channels in the immediate vicinity of the nanoparticle.

5

10

15

20

25

Although early progress in MENP neuromodulation has been encouraging, the method is far from optimized, and much remains unknown about best practices for the nanoparticles and driving fields. Much of the particle-neuron dynamic is governed by non-linear behaviors, between the threshold-based neural action potentials, complex physics of nanoparticle surface interaction, and nanoscale dynamics of the extracellular microenvironment. The complexities have meant that existing studies have largely focused on secondary measurements of increased activity and can only utilize globally excitatory biological mechanisms. Hence, the purpose of this study is to understand how the MENPs' non-linear physics needs to be exploited for controlling local electric fields in the nanoparticles' vicinity in cellular microenvironment, in turn enabling local activation or inhibition of action potentials on demand via application of magnetic fields of specific spatiotemporal profiles. However, before going into the description of this current study, it is important to give a brief overview of the past experiments conducted in our own laboratory as well as in other independent laboratories and point out their key shortcomings.

It should be noted that nearly all existing studies have relied on MENPs of "spherical" shapes, i.e., having no visible shape anisotropy. For example, in the study by Kozielski et al, they injected approximately 100 μg of CoFe<sub>2</sub>O<sub>4</sub>@BaTiO<sub>3</sub> MENPs into the subthalamic region of naïve mice to induce specific behavioral changes via simultaneous application of a relatively large biasing DC magnetic field, on the order of 2 KOe, and a relatively small AC magnetic field, on the order of 60 Oe at 140 Hz <sup>28</sup>. The spherical MENPs with a diameter on the order of 200 nm were significantly larger than the membrane thickness. In another study by Nguyen et al, they used smaller size

CoFe<sub>2</sub>O<sub>4</sub>@BaTiO<sub>3</sub> MENPs, in the sub-100-nm size range, also of a spherical shape, to evoke fast neuronal response in cortical slices ex vivo. The evoked cortical activity upon application of a low-strength AC magnetic field, on the order of 400 Oe at a sub-100-Hz frequency, was measured via two-photon and mesoscopic imaging of calcium signals and also through an increased number of c-Fos expressing cells after stimulation <sup>27</sup>. In a different study by Jang et al, they administrated approximately 100 µg/ml of sub-50-nm CoFe<sub>2</sub>O<sub>4</sub>@BiFeO<sub>3</sub> MENPs, also of a spherical shape, into ex vivo brain slices of transgenic Alzheimer's Disease (AD) mouse model. Then, they used the magnetoelectric effect to substantially dissociate Alzheimer's β-amyloid aggregates – a major pathological hallmark of AD - by application of low-frequency (<1 KHz) low-strength (~150 Oe) AC magnetic fields <sup>44</sup>. It can be noted that in all these and other past experiments, there were two major roadblocks that made it difficult to fully benefit from the main advantage, i.e., the magnetoelectric effect, of the MENP stimulation – otherwise a very promising neuromodulation approach.

5

10

15

20

25

First, arguably, the most outstanding roadblock was due to the lack of focus to ensure the nanoparticles were being brought and remained in direct contact with the cellular membrane during the modulation process. As a result, given that the dominant portion of the cellular microenvironment is occupied by electrically conductive intracellular/extracellular spaces, most nanoparticles would statistically end up in the conductive intracellular and/or extracellular spaces. In this case, the dipole electric fields generated by MENPs would be screened out by free ions in the conductive space <sup>45</sup>, thus rendering the MENP neuromodulation ineffective. In contrast, the very few nanoparticles that statistically are in direct contact with the membrane could generate relatively strong electric fields across the dielectric membrane. Hence, only these minority nanoparticles would significantly contribute to the useful field-controlled modulation effect, thus making the implementation relatively ineffective. Indeed, according to the basic physics of

electromagnetism, the difference between the electric fields generated by the nanoparticles across the membrane in these two cases would be orders of magnitude <sup>46</sup>. The underlying physics is illustrated in Supplementary Materials Fig. S1.

The second roadblock in these past studies was caused by not exploiting the highly non-linear physical properties of the magnetic core of the core-shell MENPs, e.g., the M-H hysteresis loop. Arguably, the most common approach was to apply a relatively high DC bias field, on the order of the coercivity field, followed with application of a relatively small AC magnetic field, thus triggering only a differential response of the magnetization, in turn leading to a relatively small induced AC electric field <sup>28</sup>. This approach might be adequate for the nanoparticles' characterization, e.g., to measure the differential reversible ME response 40, however, it is not adequate for the high-efficacy neuromodulation application, when the highest possible (nondifferential) electric field response needs to be evoked <sup>26</sup>; thus, the non-linear M-H characteristic, involving a full hysteresis loop, must be exploited. Only then, reversible control of neural modulation would be feasible. Furthermore, as discussed below in more detail, to fully leverage the ME effect, the applied field needs to be normalized to the nanoparticle' intrinsic anisotropy field rather than to its extrinsic coercivity field. To overcome these two shortcomings, this study used rectangular-prism-shaped nanoparticles, with well-defined shape and magnetocrystalline anisotropy, with surface functionalization and field conditions required to improve the nanoparticle-membrane surface interface and leverage the above non-linear physics of the magnetic cores.

#### **RESULTS**

20

5

10

## Synthesis of alternative shape Magnetoelectric Nanoparticles

5

10

15

20

To maximize the conversion of the magnetic field energy into local electric fields to directly modulate neural activity, the MENPs' ME effect needs to be improved through optimized synthesis. The details of synthesizing core-shell magnetoelectric nanoparticles following a wetchemical approach are described thoroughly in <sup>26,40,47</sup>. In brief, magnetostrictive cores of cobalt ferrite are coprecipitated and then coated in barium titanate through thermal decomposition. This approach generally gives high fidelity over nanoparticle shape and size and a narrow band of nanoparticle properties. The previously described synthesis approaches have largely produced spherical nanoparticles, as crystal growth mechanics in that setting favors isotropic growth that minimizes free surface area. However, several recent papers have noted that other nanoparticle shapes have theoretical advantages in field generation<sup>48</sup>, and our previous studies have already demonstrated significant changes in the magnetoelectric properties of nanoparticles based on modifications of the nanoparticle cores <sup>49</sup>. Additionally, previous in vivo studies have indicated that there is a drop off in stimulation efficacy after long trains of pulses that diverges from equivalent electrode methods <sup>50</sup>. We've theorized that the nanoparticles might separate from the neuron membrane during stimulation, as they're attached only by electrostatic forces. These forces are modified by the magnetoelectric effect, and the gradient magnetic field imparts a relatively small amount of force on the nanoparticles as well. The magnetoelectric effect generated by the nanoparticles drops off strongly with distance, both due to the loss in electric field flux and screening effects from the highly mobile ions in neuronal environments. As such, it is critical to determine a way for the nanoparticles to sit on the membrane that goes beyond more typical chemical attachment- and size-based mechanisms, which can greatly change clearance rates that matter for clinical applications<sup>34,35</sup>. To do so, in this study, we have attempted to promote anisotropic growth in the nanoparticles, targeting a flatter rectangular prism shape with an

increased drag coefficient (Fig. 1). To achieve this, we have taken advantage of the role of sodium hydroxide as the precipitating agent (see Methods and Supplementary Materials Fig. S3 and Fig. S4). In a typical synthesis, sodium hydroxide works to shift the reaction to favor cobalt ferrite over the otherwise energetically preferably magnetite and to promote the formation of inverse-spinel phases over cubic and spinel phases. However, as pH reaches 12+, sodium hydroxide also inhibits the formation of cobalt ferrite, slowing down the growth and leading to smaller, more crystalline nanoparticles. Keeping the nanoparticles small is critical to clinical applications that require traversing the blood brain barrier <sup>51,52</sup>. Keeping the nanoparticles crystalline is important for maximizing the vital lattice-matched surface interface between the core and the shell. The resultant nanoparticles have displayed a highly anisotropic shape with clear preferential growth axes (Fig. **3A)**. Raw transmission electron microscopy (TEM) images are also shown in Supplementary Materials Fig. S5 and Fig. S6. Composition images acquired via HRTEM-EDX are shown in Supplementary Materials Fig. S11. Cores had a magnetic saturation of 20.32 emu/g and coercivity of 912Oe, with an anisotropy field on the order of 9 KOe. After the shell addition, the saturation magnetization and the coercivity field have changed to 0.74 emu/g and 325 Oe, respectively (Fig. 3B).

5

10

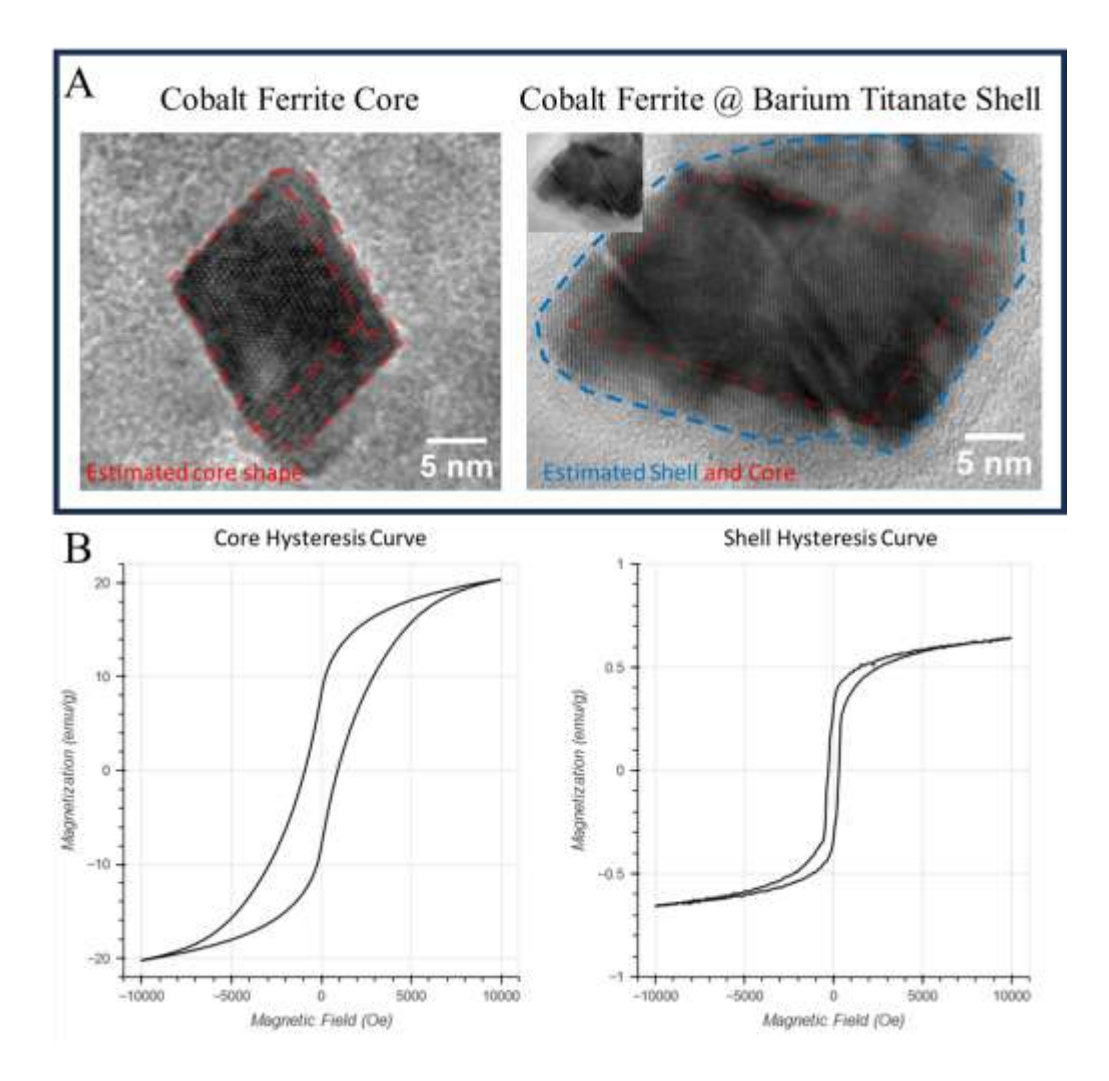


**Figure 3: MENPs characterization:** (**A**) TEM image showing (left) the core of a rectangular prism shape and the (right) fully-enclosed core-shell nanostructure of MENP. The ferrimagnetic spinel CoFe<sub>2</sub>O<sub>4</sub> magnetostrictive core is surrounded by the perovskite BaTiO<sub>3</sub> piezoelectric shell. Original image (insert) and estimated core-shell structure (highlighted with dotted red and blue lines, with the blue line marking the interface) are shown. (**B**) M-H loops of the cobalt ferrite cores (left) and the core-shell MENPs made of these cores under study, measured via a Lakeshore alternating gradient magnetometer Mircomag 2900. The MENP's coercivity field, H<sub>c</sub>, is on the order of 0.5 KOe, the saturation magnetization, M<sub>S</sub>, is on the order of 0.7 emu/g. A field on the order of 2 KOe is required to saturate the magnetization.

#### Strong stimulation response from alternate shape MENPs

5

10

15

To test the MENPs' ability to stimulate neurons via magnetic field application, a series of in vitro experiments has been conducted on hippocampus cell cultures grown from Sprague Dawley embryonic day-18 rat neurons. To detect neural activity, cell cultures under study have been tagged

with Cal-520 – a Ca2+ sensitive fluorescent dye from AAT Bioquest. Cal-520 has been chosen for its fast transient response and insensitivity to magnetic fields <sup>53</sup>. The MENPs were coated with a thin layer of polyethylene glycol (PEG) (~MW 1500) and thoroughly sonicated immediately prior to administration (0.5 mg of MENPs per 100,000 cells) into the cell culture. The PEGylation improves particle dispersion, which is critical to ensure a maximization of ME effect and to ensure nanoparticles can adhere to the cell membrane (**Fig. 2**). This is because agglomerates tend to be spherical to minimize surface energy, which leads to randomly oriented polarization and poor

5

10

15

20

contact area.

The dielectric membrane is the "gate" that separates the conductive intra- and extra-cellular spaces. This membrane "gate" is made of densely placed ion channels. The ion channels, regulated by local electric fields, control the flow of ions across the membrane to maintain the charge balance required for neural firing or inhibition. Placing the nanoparticles on the membrane effectively makes them an integral part of the membrane, in turn allowing to directly control the membrane "gate" via externally applied magnetic fields <sup>46</sup>. In this case, the applied magnetic fields need to match the non-linear M-H hysteresis loop of the nanoparticles (**Fig. 3B**). Particularly, it is important to ensure the AC field amplitude significantly overcomes the coercivity of the nanoparticles, as discussed below in more detail. The non-linear M-H physics that underlies the selection of the applied magnetic field strength is described in Supplementary Materials **Fig. S2**.

A typical image of a cell culture obtained with a fluorescent optical microscope using a 20X lens is shown in **Fig. 4A**. As an example, a typical field-controlled neuronal activity for the same cell culture with MENPs is shown in an overlayed fluorescent image in **Fig. 4B**. The activity prior to and during stimulation is shown in cyan and red colors, respectively. Each experiment consisted

of three phases including baseline, stimulation, and post-stimulation, respectively. A stimulation run consisted of two-second pulses of an applied magnetic field (1.7kOe 50Hz), followed by 28 seconds without field, repeated 3-4 times in a single experiment. Approximately 90 seconds of baseline activity and 30 seconds of post stimulation activity were recorded before and after each experiment for use in control comparisons. Additional controls consisted of repeat experiments at lower strength fields (1.2 KOe, 1.4 KOe), and a high field (1.7 KOe) stimulation experiment conducted prior to the addition of MENPs. The experimental setup is shown in **Fig. 4C**. The experimental design and reasoning are explained in greater detail in *Methods*. A characteristic video is shown in the enclosed Supplementary Materials **Movie S1**.

5

10

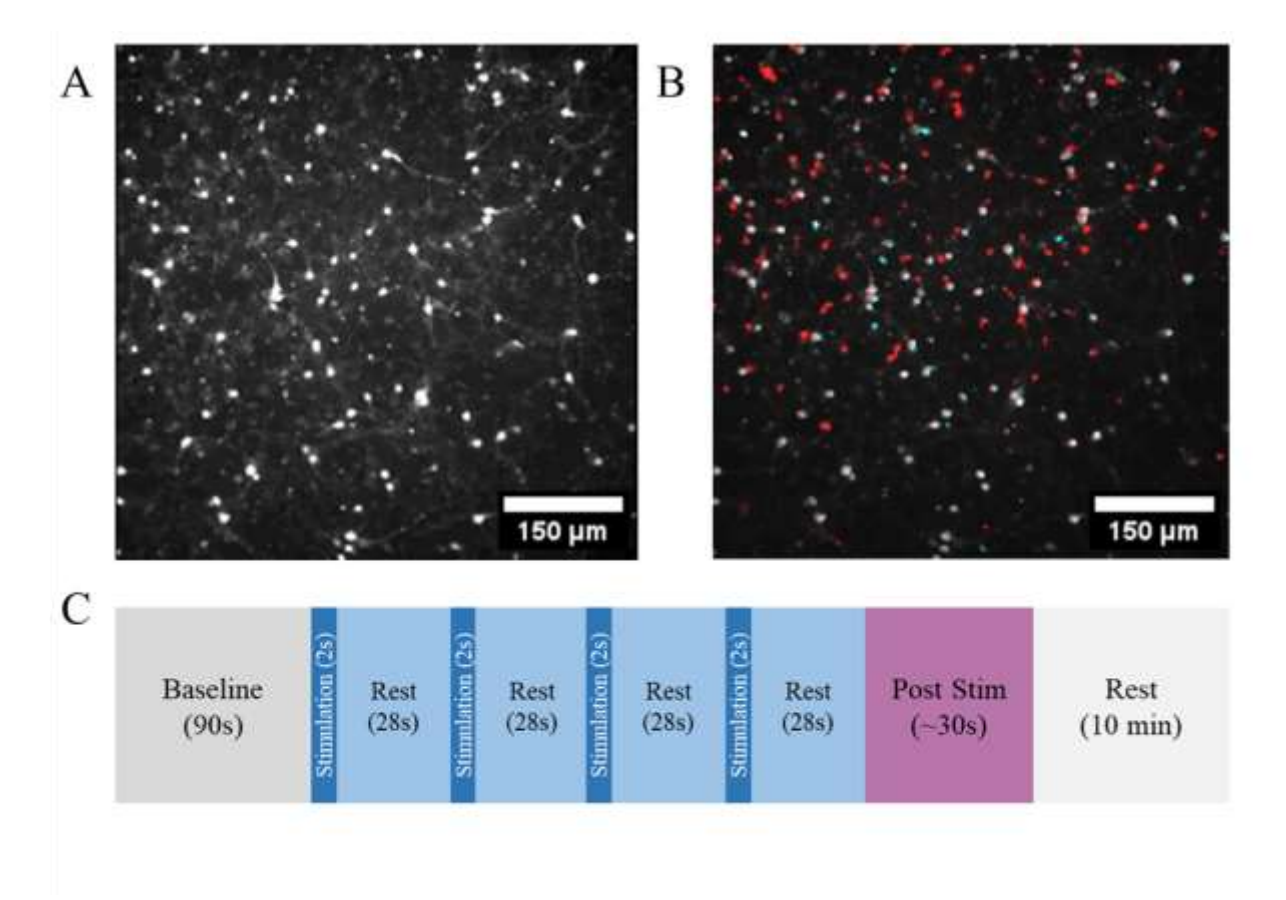


**Figure 4: Experimental methods and design.** (A) Typical 20X microscopy image of Cal-520 dye treated neurons. (B) 20X microscopy image with fluorescent overlay of firing activity. Cyan for activity occurring before stimulation and Red for activity occurring during stimulation. (C) Standard experiment design, with 90s of baseline firing rate recording followed by 3-4 pulses of 50Hz signal lasting two seconds each and separated by 28 seconds of rest.

At least 30s of additional post-stimulation baseline following the end of stimulation were recorded.

A sample time trace is shown in **Fig. 5**.

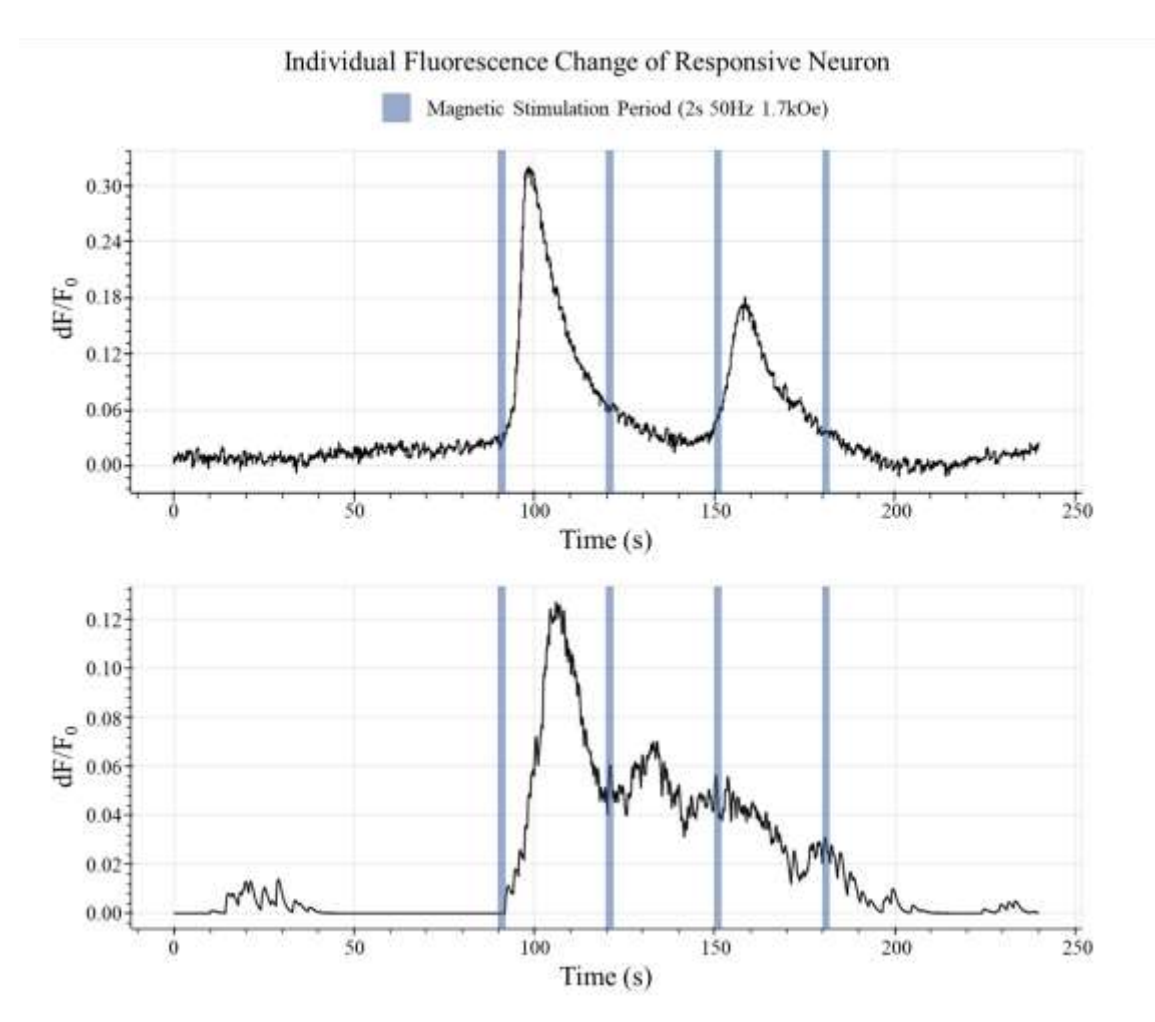


Figure 5: Single denoised and detrended time trace of a responsive neuron. Raw fluorescence traces extracted using imageJ then fed through denoising and detrending pipelines to create isolated traces.

5

10

All experiments show statistically significant increases in neuron firing activity (P < 0.01, linear mixed effect models controlling for neuron location (LME)) compared to baseline activity rates. To make sure that the activity changes are not due to random fluctuations in synchronized firing, we have compared equivalent time periods in baseline in all experiments and found no significant

changes in neuron activity (P > 0.05, LME). 87.5% of stimulation events have produced a significant change in neural activity (P < 0.05, LME), with 58.3% of stimulation events producing a strongly significant change in neural activity (P < 0.01, LME). Furthermore, post stimulation periods have not generally shown significant changes compared to their paired last stimulation period, with only one experiment showing statistically significant differences (P < 0.05, LME). Without nanoparticles, no stimulation events have produced significant changes in activity (P > 0.15, LME). A summary of statistical significance data is shown in **Table 1**, also summarized in Supplementary Materials **Fig. S7**. Stimulation typically causes 20-30% of neurons to fire compared to baseline activity rates. Changes in activity rates across all experiments are shown in **Fig. 6**. Additionally, unlike our previous studies using traditional spherical MENPs  $^{26}$ , neurons have remained at enhanced activity rates for a few seconds following stimulation, depending on the stimulation pulse (Supplementary Materials **Fig. S8**).

5

10

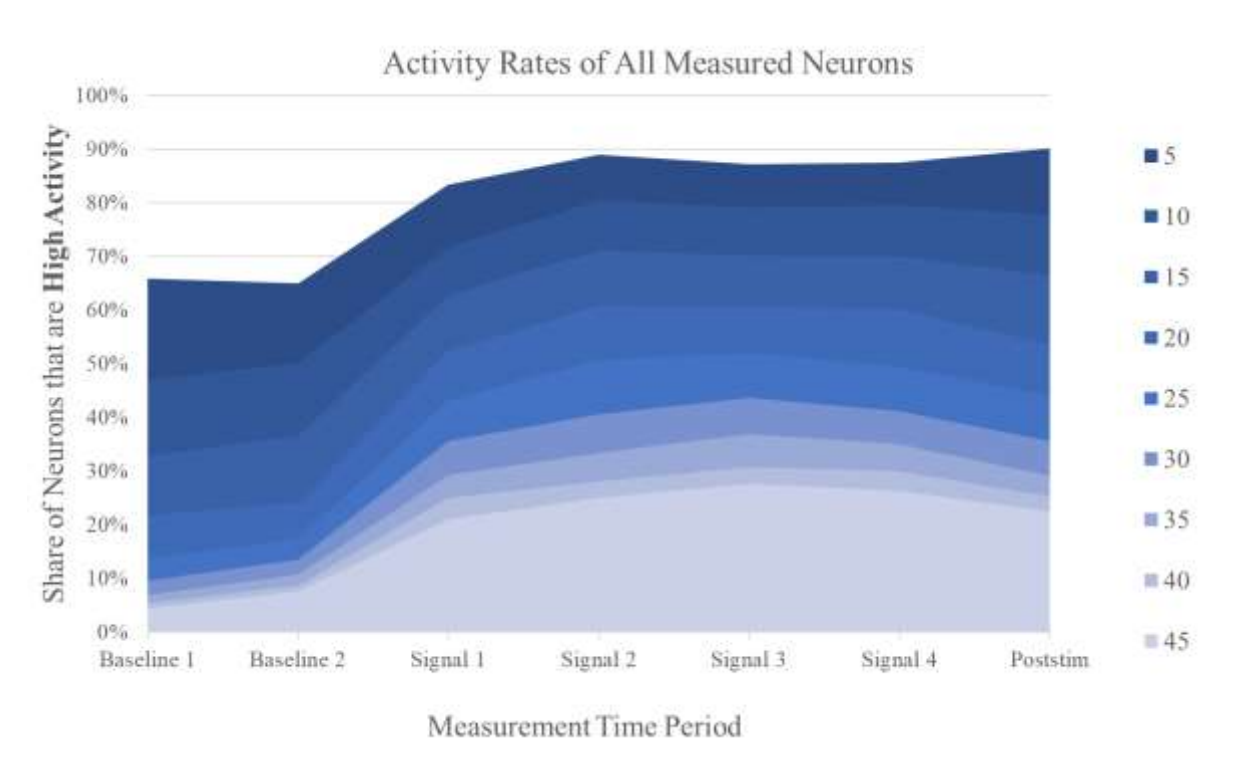


Figure 6: Change in activity rates across signal period. Summary data of all neurons (n = 2446). Various levels of measured activity rate (action potentials per 30s period) used as comparison

points. First and second stimulation pulses tended to produce the largest gains over baseline activity. Post stimulation activity is typically lower than the peak during stimulation.

Table 1: Summary of statistical significance in comparative time periods. P-values for all Linear Mixed Effects models comparisons between different baseline and signaling time periods. Red borders indicate when experiments are separated by an applied DC field. Notably, none of the control periods (Baseline 1 vs Baseline 2) experienced significant changes in neural response. Similarly, only one experiment saw a significant change in neural activity following the cessation of applied field (Signal 4 vs Post Stim).

| Comparison Periods       | No Particles $n = 785$ |       | $\operatorname{Exp} 2$ $n = 251$ | Exp 3 $  n = 325$ | Exp 4 $n = 324$ | Exp 5 $  n = 332$ |       |
|--------------------------|------------------------|-------|----------------------------------|-------------------|-----------------|-------------------|-------|
| Baseline 1 vs Baseline   | 2 0.389                | 0.261 | 0.228                            | 0.075             | 0.059           | 0.235             | 0.697 |
| Baseline 2 vs Signal 1   | 0.555                  | 0.003 | 0.003                            | 0.013             | 0.044           | 0.014             | 0.129 |
| Signal 1 vs Signal 2     | 0.388                  | 0.017 | 0.005                            | 0.001             | 0.011           | 0.007             | 0.006 |
| Signal 2 vs Signal 3     | 0.187                  | 0.270 | 0.021                            | 0.001             | 0.001           | 0.017             | 0.001 |
| Signal 3 vs Signal 4     | N/A                    | 0.412 | 0.005                            | 0.001             | 0.000           | 0.003             | 0.000 |
| Last Signal vs Post Stin | n 0.187                | 0.412 | 0.141                            | 0.104             | 0.089           | 0.127             | 0.034 |

## Field strength and frequency modulates neuron response

5

10

15

20

During previous experiments, we have observed that the firing activity of neurons was typically lowest at the start of experiments, which contrasted with our understanding of calcium decay dependent apparent firing rates and differed from our in vivo data indicating higher baseline activity rates after nanoparticle injection and before stimulation <sup>27</sup>. One potential explanation was that during in vitro experiments, we use a gradient DC field after adding nanoparticles to the neuron dishes to draw the nanoparticles off the surface of the media and onto the neurons (see methods). This DC field would cause the nanoparticles to enforce a constant and highly directional polarization field, thus breaking the spherical symmetry of the typical neural activation process. Other studies performed on neurons have shown inhibitory effects of DC electric fields <sup>54,55</sup>.

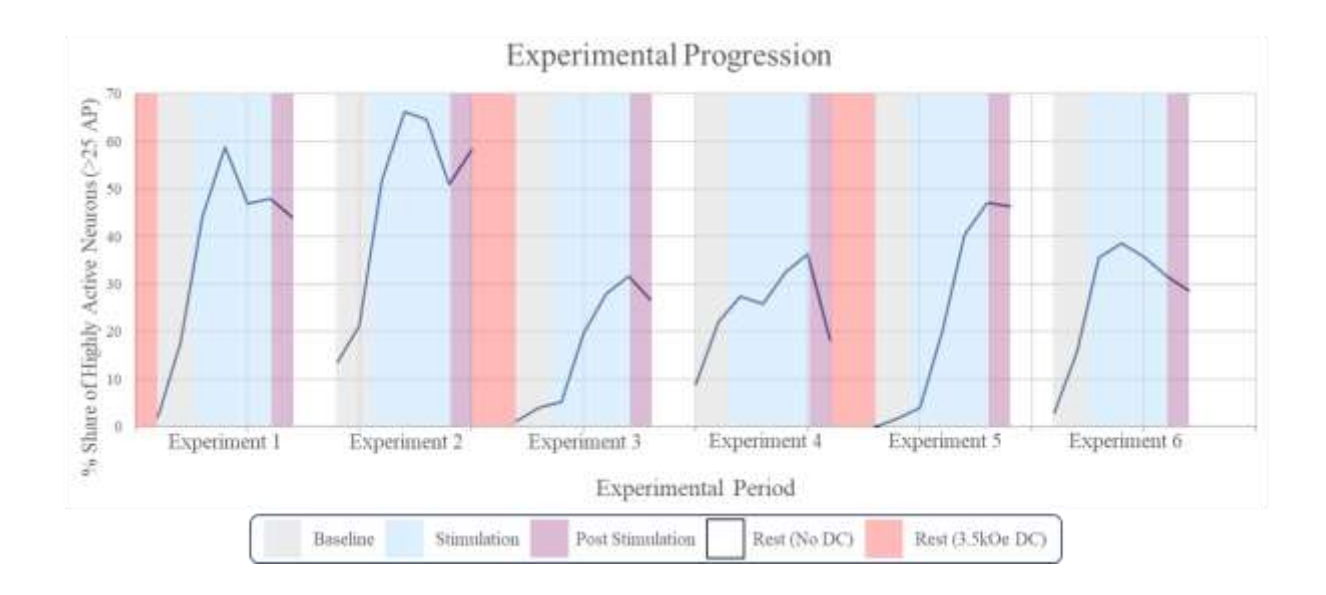


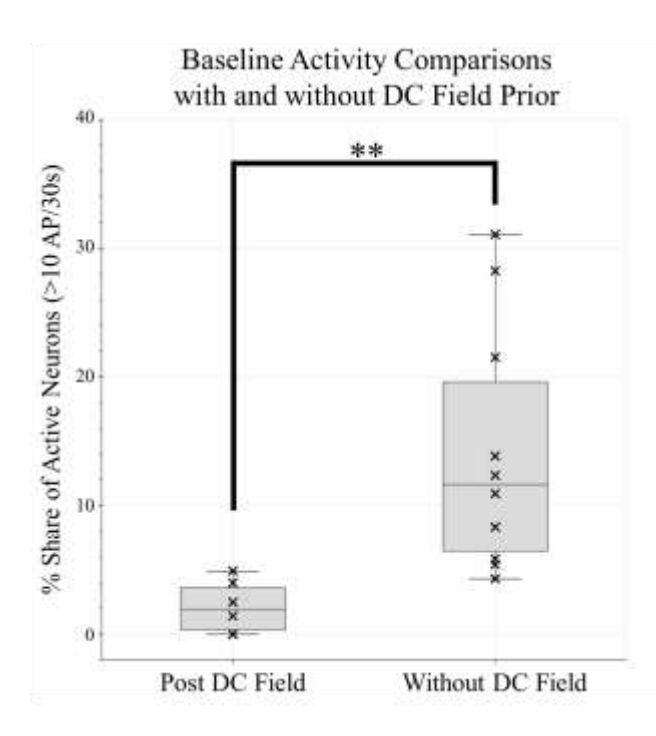
Figure 7: Using AC and DC magnetic fields to wirelessly control excitation and inhibition of neural activity. Plot of variation in number of neurons that experience highly active periods (firing in excess of 25 times per 30 seconds) over time. Rest between stimulation trains alternated between no field and high DC field (3.5 kOe) shown in red. The application of DC field appears to suppress starting baseline activity (grey) in experiments 1, 3, and 5.

10

15

20

To test this, we performed an exploratory analysis of the DC effect by alternatingly applying low-gradient DC field (3.5 kOe) or no field between MENP AC stimulation events and recorded the baseline activity rates immediately after for comparison. The experimental pattern and change in activity rates are shown in **Fig. 7.** Following DC inhibition, only 2.14% of neurons demonstrated notable spontaneous firing activity (>10 action potentials in 30s time period). Whereas a significantly larger 14.19% share of neurons were active during baseline without DC inhibition (p = 0.0096, Student's t-test). A comparison of their distributions is shown in **Fig. 8.** Furthermore, the first stimulation following DC inhibition tended to activate proportionally far more neurons relative to first stimulation pulses without DC inhibition prior (423.21% increase in active neurons vs 31.79% without DC inhibition), although the percentage of active neurons was still higher in the non-DC case (25.07% vs 17.62%).



10

15

Figure 8: Baseline activity rates with and without DC inhibition. Distribution of baseline action potential rate for experiments following 10 minutes of DC inhibitory field (n = 6) versus 10 minutes of zero field (n = 10). The ratio of the applied magnetic field strength to the nanoparticles' anisotropy field is used as a wireless "On/Off" modulation switch.

We additionally explored whether the strength of the applied magnetic field can modulate the type of neural responses. In previous studies, we saw significant drop off in stimulation effectiveness if the applied magnetic field fell far below the MENP's coercivity field in the sub 100Hz frequency domain <sup>26</sup>. Studies by other groups have achieved success with sub-threshold fields when applying an AC field while using a DC field for biasing <sup>28</sup>. To understand how the neuromodulatory effects vary with field strength, we lowered the applied field from a maximum of 1.7 KOe to 1.0 KOe as well as a control case without applied field. This approaches the coercivity field of approximately 0.5 KOe for the MENPs used in these experiments. The average neural responses to the first pulse of each of these field strengths are shown in **Fig. 9**.

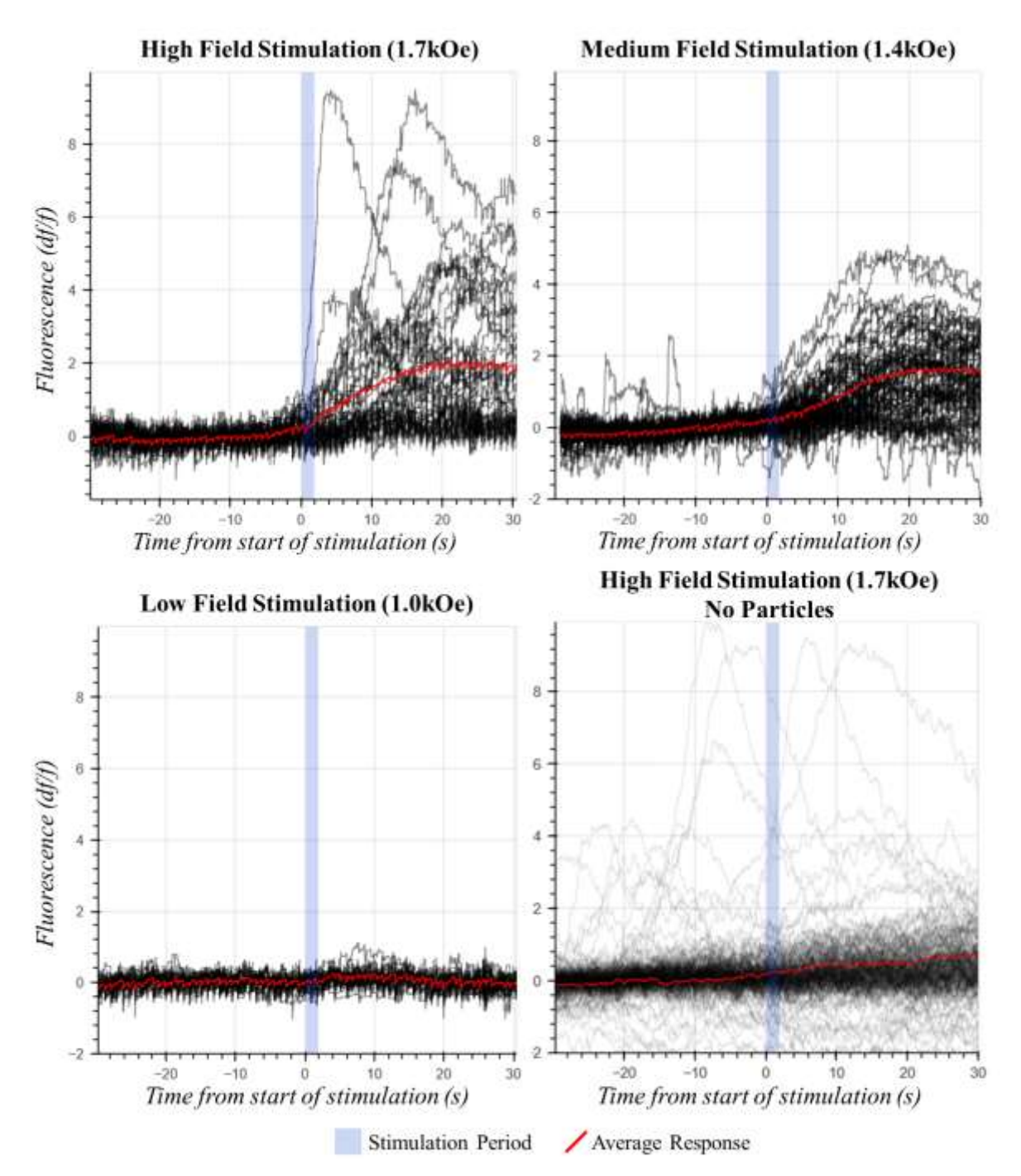


**Figure 9: Pulse triggered average fluorescence activity at different stimulation field strengths** (1.7, 1.4, 1.0 KOe). Neuron pulse-triggered averages of the magnetic pulses from responsive neurons (n > 300) for each of the attempted field strength conditions during the *first* application of field. The shaded region corresponds to the duration of the applied signal. Prior to the applied field, each measurement was preceded by approximately 10 minutes of time without any stimulation to allow firing to return to baseline levels.

10

Observationally, high field (1.7 KOe) stimulation produced both larger and sharper changes in fluorescence in some neurons. Medium field (1.4 KOe) stimulation did not produce as many instantaneous large shifts in fluorescence but produced similar average change compared with high

field. Low field (1 KOe) stimulation did not produce noticeable changes in neuron behavior in the first pulse, which matches statistical data indicating that the fourth pulse in low field conditions tended to be the most impactful.

#### **DISCUSSION**

5

10

15

20

25

These experiments demonstrate that MENPs can controllably induce and even inhibit action potentials on demand via application of AC and DC magnetic fields, respectively. However, to achieve such control, it is necessary to exploit the highly non-linear properties of these core-shell nanoparticles, e.g., due to the core's M-H hysteresis loop. In general, the MENP neuromodulation is defined by the nanoparticles' physical properties such as the ME coefficient and the magnetocrystalline anisotropy field. The ME coefficient determines the strength of the wirelessly controlled modulation, while the anisotropy field defines a wirelessly controlled "On/Off" switch of the modulation. The applied magnetic field's strength and frequency need to relate to the nonlinear properties of the core. In fact, the dependence of the neuromodulation efficacy has an exponential dependence on the applied field strength and frequency (Fig. S2 and Fig. S9). That is why, given the cobalt ferrite core's anisotropy field on the order of 10 KOe, application of magnetic fields with strengths below 1.4 KOe showed reduced modulation effects at 50Hz. It is notable that the coercivity field over these nanoparticles (averaged over orientations) is on the order of 0.5 KOe, i.e., significantly smaller than the anisotropy field, on the order of 9KOe. The coercivity field is an extrinsic field that is a fraction of the intrinsic anisotropy field. It defines the reversed field at which the average magnetization turns to zero in the full M-H hysteresis loop. In an ideal single-domain uni-axial anisotropy approximation, the full M-H hysteresis loop of a nanoparticle could be described by the Stoner-Wohlfarth model <sup>56</sup>. The coercivity field depends on the quality of the magneto-crystallinity and the nanoparticles' shape as well as the relative orientation of the applied magnetic field with respect to "easy" axes defined by the magetocrystalline anisotropy energy of the core. As a result, this field also depends on the

10

15

20

measurement time. For example, the M-H loop, i.e., the irreversible part of the M-H curve, would entirely disappear if the measurement time was infinitely long. In this study, the M-H loop was measured for a large collection of MENPs, implying that the loop was averaged over all the relative orientations of the applied field. Assuming the nanoparticles are uniformly distributed over the membrane surface and the average neuron has a spherical shape, not all the nanoparticles would have their magnetization aligned along the applied field at the coercivity value. In a rough estimate, approximately less than 5 and more than 50% of nanoparticles would fully align their magnetization along the field, given the applied field of less than 1 KOe and more than 1.7 KOe, respectively. According to the M-H hysteresis loop, a field above 2 KOe would be required to saturate the magnetization. In turn, because the core's magnetization is directly coupled to the piezoelectric shell's polarization, the polarization cannot undergo a relatively significant change unless the applied magnetic field substantially exceeds the coercivity field, with the maximum effect occurring when the field exceeds the saturation field. This explains a more pronounced firing response in the case of 1.7 KOe, compared to the 1 KOe field case. The physics of the magnetization reversal based on the applied field's strength is based on the interplay of major and minor M-H hysteresis loops, as discussed previously and illustrated in Supplementary Materials Fig. S2 <sup>26</sup>. Ideally, assuming the nanoparticles became an integral part of the neuronal membrane and there were enough nanoparticles to deliver sufficient energy locally, the probability of (wirelessly) inducing stimulation of local neural activity would be equivalent to the probability of switching the magnetization by a magnetic field. Then, simplifying the magnetic anisotropy of the average nanoparticle as having a cylindrical symmetry <sup>57</sup>, the probability of local neural firing, P, could be estimated by this expression:

$$P \sim \exp\left(-\frac{KV}{k_BT} \left(H_S - H\right)/H_S\right),\tag{2}$$

where H<sub>S</sub> is the characteristic field that is required to saturate the average nanoparticle in the system, H is the applied field, K and V are the core's magnetic anisotropy and volume, respectively,  $k_B$  is the Boltzmann constant, and T is the ambient temperature. Indeed, assuming the average saturation field of 1.9 KOe, the characteristic MENPs' core size on the order of 8 nm, the anisotropy of the cobalt ferrite on the order of 10<sup>6</sup> J/m<sup>3</sup>, this theoretical expression seems to adequately explain the probability of firing extrapolated from the above experiments at the four applied field values, 0, 1, 1.4, and 1.7 KOe, respectively (Fig. 9). The theory-experiment comparison is shown in Fig. S9. However, though the effect observed in this experiment under application of a magnetic field of 1.7 KOe is noticeable, not all the nanoparticles are likely to contribute to the net signal. To involve all the nanoparticles, the applied field needs to exceed the saturation field, in turn scaled to the anisotropy field. Therefore, in the future, with the goal to maximize the modulation efficacy, two alternative ways to achieve full alignment of the magnetization could be pursued: (i) increase the applied field to exceed the anisotropy field or (ii) substitute the cobalt ferrite core with a magnetostrictive material with the anisotropy field reduced to approximately 1 KOe, thus making it comparable with the relatively small applied field. The latter could be achieved, for example, by substituting cobalt ferrite with nickel ferrite as the core material <sup>40</sup>.

5

10

15

20

Besides the above argument of scaling up the applied field to the intrinsic magnetocrystalline anisotropy field, the reason that MENPs can modulate neural activity is also because the rectangular-prism-shaped nanoparticles (versus the traditional spherical shaped MENPs) meet the following two requirements. First, the nanoparticles are prepared to have the highest possible magnetoelectric coefficient, on the order of 1 V/cm/Oe. The goal is accomplished not only by

maximizing both the core's magnetostriction coefficient and the shell's piezoelectric coefficient but also by improving the interfacial lattice match between the core and the shell through maximizing the "useful" interface surface area and accordingly reducing the thickness of the nanoparticle, thus creating a rectangular prism shape. The detailed synthesis process, aimed to meet the requirements by providing relatively high-quality crystallographic nanostructures, is described in Methods. It can be noted that the high-quality crystallographic nanostructure of a rectangular prism shape also leads to a relatively large surface area between the membrane surface and the nanoparticle's side interfacing the surface. Second, coating the nanoparticles' surface with a relatively thin PEG layer has a two-fold purpose: (i) minimize the potential agglomeration of nanoparticles, thus improving the overall dispersion and maintaining the required nanoscale physics and (ii) maximize the likelihood of the nanoparticles to "stick" to the membrane via the Van-der-Waals force, thus substantially increasing the local electric field generated by the nanoparticles due to their magnetoelectric effect. Regarding the latter, it should be remembered that the electric field generated by MENPs across the membrane when the nanoparticles are in direct contact with the dielectric membrane could exceed 1000s V/cm, i.e., orders of magnitude larger compared to the case when the nanoparticles are in the conductive intra- or extra-cellular spaces (Fig. S2) 46. Indeed, for the latter, the nanoparticles' electric fields would be screened out by free ions in the spaces to below 1 V/cm, with the effective Debye length in the sub-1-nanometer size range 45,46.

20

5

10

15

The fact that during each measurement time, the calcium signal did not fully relax back to the initial pre-excitation state can be partially explained by a relatively slow response of this particular fluorescent dye <sup>53</sup> and also by the fact that at this early stage of research the nanoparticles had a relatively large size distribution. The underlying physics is described in more detail in the Methods

section below. According to this physics consideration, the above problem can be overcome through engineering nanoparticles of the right size with a sufficiently narrow size distribution.

5

10

15

20

To further highlight the fundamental nature of this wireless neuromodulation approach and demonstrate its future potential, we conducted a preliminary experiment to explore whether the application of a DC magnetic field could locally inhibit neuron excitations. At the current time, we can only demonstrate correlation between lower firing rates and the application of DC fields, but the effect deserves further, more dedicated study. The functional mechanism behind DC MENP inhibition is challenging to determine, in part because the mechanism behind stimulation is also currently debated. Our previous work indicated that it was ion channel mediated as selective inhibition of sodium channels successfully blocked MENP stimulation, but we're uncertain whether this extends to DC inhibition. From the nanoparticle physics perspective, we do know that while under constant DC magnetic field, the particles should exhibit constant DC electric field. However, unlike electrode systems, the field lines curve sharply and are extremely local to the particle, creating high gradients. Furthermore, the DC electric field is not evenly distributed across neuron, which is a scenario that does not have an analog in electrode stimulation. These differences complicate our understanding of DC MENP inhibition, as it is unclear to what degree insights gained from DC electric field inhibition, which has been demonstrated by other groups, would apply to MENPs. Given that, we have come up with a few scenarios that could be possible. First and foremost, we would start from the assumption that MENP inhibition follows similar mechanisms to electrode inhibition, in that the strong directional electric field can interrupt the free flow of ions as an action potential propagates. This disruption prevents the continuous propagation of an action potential around the nodes of Ranvier. To test this, we would want to see whether there was a polarity-direction dependence between the inhibitory effect and the DC field.

Another possibility is that the shielding effect discussed earlier that draws ions in solution to the surface of the MENPs might locally deplete the number of available ions in the extracellular space for cell signaling. A third possibility is that the DC electric field saturates the ion channels, interrupting the process by which they restore internal/external ion concentrations back to resting potential. One of the considerations is whether there is a hypothetical difference between the mechanisms triggered by application of AC and DC magnetic fields, based on breaking the spherical symmetry of the typical neuronal activation. A conceptual diagram is illustrated in Supplementary Materials **Fig. S10**. Application of a DC field significantly increases the membrane potential on one half of the cell only, thus effectively excluding this half of the cell from contributing to the collective energy generation required for triggering an action potential. This collective effect scales with the characteristic time of ion channel activation, ranging from a millisecond to tens of milliseconds <sup>58</sup>. Hence, the DC field needs to be applied for longer than tens of milliseconds for the inhibition mechanism to work.

5

10

15

20

In summary, besides maximizing the magnetoelectric effect and applying a magnetic field determined by the anisotropy field of the magnetostrictive core, it is difficult to overestimate the significance of placing MENPs directly on the membrane, whether it is by creating the right shape or functionalizing them with special membrane targeting biomolecules. In addition, it can be noted that if these conditions are met, MENPs would require orders of magnitude smaller densities, e.g., < 1 µg, instead of 100s µg, per dish of 100,000 neurons, compared to stimulation approaches using other nanoparticles, to achieve modulation with signals comparable to those of optogenetics, thus not causing any toxicity concerns <sup>39,44,59</sup>. Therefore, MENPs pave a way to establish a wireless control of local neuromodulation via application of magnetic fields. The wireless control knobs

are determined by the applied magnetic field's strength and frequency, in turn defined by the nanoparticles' highly non-linear properties such as the core's M-H loop.

#### 5 **Methods**

10

30

35

45

Nanoparticle synthesis

#### Chemicals:

Cobalt(II) Nitrate Hexahydrate<sup>SA</sup> (Co(NO<sub>3</sub>)<sub>2</sub>•6H<sub>2</sub>O), Iron(III) Nitrate Nonahydrate<sup>SA</sup> (Fe(NO<sub>3</sub>)<sub>2</sub>•9H<sub>2</sub>O), Sodium Hydroxide<sup>SA</sup> (NaOH), Barium Carbonate<sup>FS</sup> (BaCO<sub>3</sub>), Titanium(IV) Isoproproxide<sup>SA</sup> (Ti[OCH(CH<sub>3</sub>)<sub>2</sub>]<sub>4</sub>), Citric Acid<sup>SA</sup> (HOC(COOH)(CH<sub>2</sub>COOH)<sub>2</sub>), Polyethylene Glycol<sup>SA</sup> (H(OCH<sub>2</sub>CH<sub>2</sub>)<sub>n</sub>OH, MW: 3000), and Ethanol<sup>MS</sup> (>99.7%), were purchased from Sigma Aldrich, Fisher Scientific, and Millipore Sigma (SA, FS, MS respectively). All reagents were used without further purification.

#### Core Synthesis:

15 Core-shell magnetoelectric nanoparticles were synthesized following a modified process described previously <sup>26,47</sup>. The cobalt ferrite cores followed a coprecipitation process using metal salts of cobalt and iron, with sodium hydroxide as the precipitating agent. In a typical synthesis, 100mg of Cobalt Nitrate and 278mg of Iron Nitrate were dissolved into separate beakers containing 20ml of DI water each under constant stirring. The beakers were brought close to the reaction temperature of 90°C and then mixed together. 3 M Sodium Hydroxide aqueous solution was added until the mixture reached a pH of 13, immediately starting the precipitation process. The reaction was allowed to evolve for 1 hour to reach the intended size of 15-20nm. The solution was then cooled, and the Cobalt Ferrite particles were separated from solution magnetically. The nanoparticles were then washed twice in DI water and once in Ethanol to remove excess reactants before drying overnight.

#### Shell Addition:

The Barium Titanate shells were formed on the Cobalt Ferrite cores at a 1:2 (core:shell) stochiometric ratio using a modified solgel and thermal decomposition process. For a typical synthesis, 50mg of the previously prepared Cobalt Ferrite cores were mixed in 20ml DI water with 500mg of Citric Acid. This beaker was then probe sonicated for two hours to fully disperse the cores. In separate beakers, 88mg of Barium Carbonate and 126µl of Titanium Isopropoxide were mixed with 20ml of DI water and Ethanol respectively. 800mg of Citric Acid then added to both the barium and the titanium beakers and allowed to mix for an hour at room temperature to ensure full chelation. These beakers were then mixed together, and the resultant solution was brought to 90°C to begin evaporating the excess Ethanol and DI water. The sonicated cores were added in once the combined barium and titanium solution reached 20ml. The final solution is then allowed to evaporate until a gel forms. The gel is then slowly heated to 800°C and kept there for 6 hours before slowly cooling back down to room temperature. The final product is ground down in a mortar and pestle and washed twice in DI water and once in Ethanol before drying overnight.

#### 40 MENP PEGylation:

MENPs were coated in Polyethylene glycol (PEG)to improve dispersion. In a typical process, 1mg of MENPs were dispersed in 1-3ml of DI water by probe sonicator for two hours to achieve a near monodisperse solution. PEG was added in excess at a 1:8 mass ratio to solution and sonicated for an additional two hours. The particles were then washed in DI water to remove excess unbound PEG before resuspending in DI water at the desired concentration.

Underlying Physics Showing Importance of MENPs Having a Narrow Size Distribution:

The MENPs' core size determines the stability ratio,  $KV/k_BT$ . In turn, the stability ratio determines the exponential time dependence of the magnetic core's non-volatility time on the size of the core  $^{60}$ 

$$\tau \propto \tau_0 e^{\frac{KV}{k_B T}},\tag{3}$$

where t<sub>0</sub> is the characteristic time constant determined by the ferromagnetic resonance of the core material, typically on the order of 1 ns <sup>61</sup>. For example, given the anisotropy of the cobalt ferrite on the order of 10<sup>6</sup> J/m<sup>3</sup>, for simplicity assuming a cubic shape, by reducing the core size from 10 nm to 7 nm would reduce the non-volatility time from over ten years to approximately 1 sec. Further reducing the size to 6 nm would reduce the time into the sub-1-msec range. Given the field frequency of 50 Hz, the characteristic measurement time is approximately 20 msec, therefore the 7- and 6-nm nanoparticles would be in the hysteretic and superparamagnetic states, respectively. Ideally, the applied field frequency and the average size of the nanoparticles can be adjusted so that the nanoparticles do not fall in the superparamagnetic state, thus maintaining their significant magnetoelectric effect. Hence, future development to improve the uniformity of these nanoparticles' size and other properties would be vital for developing clinical applications.

# Hippocampus neuron culture preparation

5

10

15

20

25

30

35

40

45

Primary neuronal cultures used for this study were sourced from E18 Sprague Dawley Rat (Brainbits) hippocampus dissociated cells. Initially untreated 35 mm petri dishes with 14 mm glass bottom culture area (Matsunami Glass D35-14-1-U) were used to improve imaging quality. The dishes were coated with 50 μg/ml poly-D-lysine (PDL) (Gibco A3890401) overnight at room temperature and rinsed three times with ddH2O and air dried. Then, 100 μg/ml laminin (BioLamina LN511) was coated on top of the PDL layer in a 37°C incubator for 1-3 hours. Dissociated cells were then seeded at a density of 60,000 cells/cm² and ½ -media change was made every 3-4 days with fresh, 37°C, CO2 equilibrated NbActiv4 (Brainbits). Experiments were conducted on the cultures between day 14 and day 21 for maximum viability.

#### Cal-520 Calcium Dye tagging

Calcium dye, Cal-520 (AAT Bioquest, Cat.# 21130), was used to record neural activity. 4.5mM stock solution was prepared in anhydrous DMSO. Dye working solution was prepared using culture media with a final concentration of 5- $\mu$ M Cal-520, and 1.5 mM probenecid (AAT Bioquest, Cat. # 20062). Probenecid was used to reduce intracellular dye indicators. Cell culture media was changed with the dye working solution and incubated in a 37°C, CO<sub>2</sub> incubator for 1 hour. Then, 5 $\mu$ g MENPs were added in the culture, gently mixed and incubated in a dark box for 30 minutes at room temperature above a 3.5kOe DC magnet.

#### *Neuron recording and processing*

Neuron fluorescence activity was recorded with a Nikon Eclipse E400 microscope. The magnet used for stimulation was mounted independently from the microscope to reduce vibrations, and both the microscope and magnet rested on an active vibration isolation optical table. AC signals were generated by a Digilent Discovery 2 board, controlled using a National Instruments DAQ device and amplified by a Class H 4000-Watt stereo power amplifier. For experiments with AC magnetic stimulation, the AC magnetic field was a 1.2-1.7 KOe bipolar square wave at 50 Hz. The electromagnets were designed according to the classical rules used to design magnetic write heads in the magnetic recording industry <sup>62</sup>. The AC field strengths were verified with a gaussmeter prior to each stimulation run. Recordings were processed in imageJ to identify neurons and extract

individual fluorescence traces. Those traces were then cleaned to remove noise and inherent calcium decay before undergoing action potential identification and deconvolution via Oasis <sup>63</sup>. Filtering was used to exclude neurons that did not fire at all over the course of the experiment. Extracted spike timings were then fed through our analysis pipeline to measure changes in spiking behavior.

## Experimental Design

5

10

15

20

25

30

35

40

45

The experimental design was as follows. For each trial, a period of 90s of "baseline" activity was recorded. This was followed by 3-4 stimulation periods, each consisting of 2 seconds of 50Hz magnetic stimulation followed by 28 seconds without magnetic stimulation. After the stimulation periods, an additional 30 seconds of "post-stimulation" activity was recorded, completing the trial. After each trial, the dish was moved to an enclosed container for a "rest period" of 10 minutes. This was intended to allow the dish to return to its original state. For half of the trials, we applied a 3.5kOe DC field during the resting period.

Regarding the DC inhibition study, the experimental design here was more complex than intended, as it was not possible with our optical set up to directly observe the activity rates during the application of DC field. Whereas the AC field could be applied outside of the field of view of the microscope, the DC magnet blocked any light from transmitting to the microscope. As such, we could not do the same sort of comparison as we had for AC stimulation. Instead, we had to measure the activity rates immediately after DC field and compare that to other periods where, excepting the DC field, all other conditions were held the same (same length of "rest" time, same storage conditions, etc.). We then measured the post-rest activity rates and compared between the trials with DC field applied and without. The DC periods were alternated with the non-DC rest periods to limit the effect that increased measurement time would have on the results (as opposed to doing all the DC trials first).

#### **Statistics**

Statistical analysis was performed in Python using NumPy, SciPy, and statsmodels libraries. Experiments followed a repeated measures design principle, and data analysis used Linear Mixed Effect Models (LME) to understand neuron behavior and account for potential synchronized grouped firing behavior in medium to high density neuron dishes. Specifically, neurons were labeled relative to their location on the dish. This location data was then used to create clusters of adjacent neurons which were treated as a random effect in the LME. When performing the linear mixed effects analysis, the spike rate of each neuron was compared against itself across the two time periods (baseline 1 vs 2 or stim 2 vs 3, etc.). Every differential comparison was then grouped together to see whether we could reject the null hypothesis. In this case, the null hypothesis was that the change in spiking rates of the population of neurons from the first period to the second is random (zero correlation with stimulation pulse). This approach with linear mixed effect models was chosen over more typical repeated measures ANOVA and linear regression to avoid assumptions of independence in the neurons, as several recent papers have noted that such assumptions can inflate p-values when neurons behave synchronously 64,65. Comparisons of independent baselines and analysis of sequential time segments were performed using Student ttest or median test for repeated measures where appropriate.

For the statistical analysis, the 90s of baseline activity was split into three 30s periods. The first period was discarded for each trial to avoid the large fluorescence drop off that occurs in the first 15 seconds of each recording due to the initial rapid Cal-520 bleaching. The remaining two time

periods (baseline 1 and baseline 2) were used as negative controls in the trials to verify that inherent firing activity was random (confirm the null hypothesis). Each subsequent time period was compared to the previous one following the LME approach. A stimulation pulse was deemed significant if it produced sufficient change in the group behavior of the neurons.

#### 5 References

15

20

- Anderson, R. J. et al. Deep brain stimulation for treatment-resistant depression: Efficacy, safety and mechanisms of action. Neurosci. Biobehav. Rev. 36, 1920–1933 (2012).
- 2. Abode-Iyamah, K. O. *et al.* Deep brain stimulation hardware–related infections: 10-year experience at a single institution. *J. Neurosurg.* **130**, 629–638 (2019).
- 3. Brandmeir, N., Nehrbass, E. & McInerney, J. An Analysis of Scalp Thickness and Other Novel Risk Factors for Deep Brain Stimulator Infections. *Cureus* (2016) doi:10.7759/cureus.792.
  - 4. Oh, M. Y., Abosch, A., Kim, S. H., Lang, A. E. & Lozano, A. M. Long-term Hardware-related Complications of Deep Brain Stimulation. *Neurosurgery* **50**, 1268–1276 (2002).
  - 5. Olson, M. C., Shill, H., Ponce, F. & Aslam, S. Deep brain stimulation in PD: risk of complications, morbidity, and hospitalizations: a systematic review. *Front. Aging Neurosci.* **15**, 1258190 (2023).
  - 6. Perlmutter, J. S. & Mink, J. W. DEEP BRAIN STIMULATION. Annu. Rev. Neurosci. 29, 229–257 (2006).
  - 7. Lefaucheur, J.-P. *et al.* Evidence-based guidelines on the therapeutic use of repetitive transcranial magnetic stimulation (rTMS): An update (2014–2018). *Clin. Neurophysiol.* **131**, 474–528 (2020).
  - 8. Schulze, L. *et al.* Cognitive safety of dorsomedial prefrontal repetitive transcranial magnetic stimulation in major depression. *Eur. Neuropsychopharmacol.* **26**, 1213–1226 (2016).
  - Sollmann, N. et al. Correlating subcortical interhemispheric connectivity and cortical hemispheric dominance in brain tumor patients: A repetitive navigated transcranial magnetic stimulation study. Clin. Neurol. Neurosurg. 141, 56–64 (2016).
  - Wagner, T. et al. Transcranial direct current stimulation: A computer-based human model study. NeuroImage
     35, 1113–1124 (2007).
  - 11. Walsh, V. & Cowey, A. Transcranial magnetic stimulation and cognitive neuroscience. *Nat. Rev. Neurosci.* 1, 73–80 (2000).
  - 12. Deisseroth, K. Optogenetics: 10 years of microbial opsins in neuroscience. *Nat. Neurosci.* **18**, 1213–1225 (2015).

- Folloni, D. *et al.* Manipulation of Subcortical and Deep Cortical Activity in the Primate Brain Using Transcranial Focused Ultrasound Stimulation. *Neuron* 101, 1109-1116.e5 (2019).
- Blackmore, J., Shrivastava, S., Sallet, J., Butler, C. R. & Cleveland, R. O. Ultrasound Neuromodulation: A Review of Results, Mechanisms and Safety. *Ultrasound Med. Biol.* 45, 1509–1536 (2019).
- 5 15. Tyler, W. J. *et al.* Remote Excitation of Neuronal Circuits Using Low-Intensity, Low-Frequency Ultrasound. *PLoS ONE* **3**, e3511 (2008).
  - 16. Violante, I. R. *et al.* Non-invasive temporal interference electrical stimulation of the human hippocampus. *Nat. Neurosci.* **26**, 1994–2004 (2023).
  - 17. Tufail, Y., Yoshihiro, A., Pati, S., Li, M. M. & Tyler, W. J. Ultrasonic neuromodulation by brain stimulation with transcranial ultrasound. *Nat. Protoc.* **6**, 1453–1470 (2011).
  - 18. Eisenberg, H. M. *et al.* MR-guided focused ultrasound pallidotomy for Parkinson's disease: safety and feasibility. *J. Neurosurg.* **135**, 792–798 (2021).

- 19. Elias, W. J. *et al.* A Randomized Trial of Focused Ultrasound Thalamotomy for Essential Tremor. *N. Engl. J. Med.* **375**, 730–739 (2016).
- 20. Krishna, V., Sammartino, F. & Rezai, A. A Review of the Current Therapies, Challenges, and Future Directions of Transcranial Focused Ultrasound Technology: Advances in Diagnosis and Treatment. *JAMA Neurol.* 75, 246 (2018).
  - 21. Chen, R., Romero, G., Christiansen, M. G., Mohr, A. & Anikeeva, P. Wireless magnetothermal deep brain stimulation. *Science* **347**, 1477–1480 (2015).
- 22. Hescham, S.-A. *et al.* Magnetothermal nanoparticle technology alleviates parkinsonian-like symptoms in mice. *Nat. Commun.* **12**, 5569 (2021).
  - Gregurec, D. et al. Magnetic Vortex Nanodiscs Enable Remote Magnetomechanical Neural Stimulation. ACS Nano 14, 8036–8045 (2020).
  - 24. Yue, K. *et al.* Magneto-Electric Nano-Particles for Non-Invasive Brain Stimulation. *PLoS ONE* **7**, e44040 (2012).
  - 25. Khizroev, S. & Liang, P. Engineering Future Medicines With Magnetoelectric Nanoparticles: Wirelessly controlled, targeted therapies. *IEEE Nanotechnol. Mag.* **14**, 23–29 (2020).
  - 26. Zhang, E. *et al.* Magnetic-field-synchronized wireless modulation of neural activity by magnetoelectric nanoparticles. *Brain Stimulat.* **15**, 1451–1462 (2022).

- Nguyen, T. et al. In Vivo Wireless Brain Stimulation via Non-invasive and Targeted Delivery of Magnetoelectric Nanoparticles. Neurotherapeutics 18, 2091–2106 (2021).
- 28. Kozielski, K. L. *et al.* Nonresonant powering of injectable nanoelectrodes enables wireless deep brain stimulation in freely moving mice. *Sci. Adv.* 7, eabc4189 (2021).
- 5 29. Ceña, V. & Játiva, P. Nanoparticle crossing of blood–brain barrier: a road to new therapeutic approaches to central nervous system diseases. *Nanomed.* **13**, 1513–1516 (2018).
  - 30. Ding, S. *et al.* Overcoming blood–brain barrier transport: Advances in nanoparticle-based drug delivery strategies. *Mater. Today* **37**, 112–125 (2020).
  - 31. Saraiva, C. *et al.* Nanoparticle-mediated brain drug delivery: Overcoming blood–brain barrier to treat neurodegenerative diseases. *J. Controlled Release* **235**, 34–47 (2016).

15

- 32. Song, H. *et al.* Multi-target cell therapy using a magnetoelectric microscale biorobot for targeted delivery and selective differentiation of SH-SY5Y cells *via* magnetically driven cell stamping. *Mater. Horiz.* **9**, 3031–3038 (2022).
- 33. Chen, X.-Z. *et al.* Magnetically driven piezoelectric soft microswimmers for neuron-like cell delivery and neuronal differentiation. *Mater. Horiz.* **6**, 1512–1516 (2019).
- 34. Pardo, M. *et al.* Size-dependent intranasal administration of magnetoelectric nanoparticles for targeted brain localization. *Nanomedicine Nanotechnol. Biol. Med.* **32**, 102337 (2021).
- 35. Hadjikhani, A. *et al.* Biodistribution and Clearance of Magnetoelectric Nanoparticles for Nanomedical Applications Using Energy Dispersive Spectroscopy. *Nanomed.* **12**, 1801–1822 (2017).
- 36. Guduru, R. et al. Magnetoelectric 'Spin' on Stimulating the Brain. Nanomed. 10, 2051–2061 (2015).
  - 37. Rao, B. N. *et al.* Investigation of magnetoelectric properties and biocompatibility of CoFe2O4-BaTiO3 coreshell nanoparticles for biomedical applications. *J. Appl. Phys.* **122**, 164102 (2017).
  - 38. Nair, M. *et al.* Externally controlled on-demand release of anti-HIV drug using magneto-electric nanoparticles as carriers. *Nat. Commun.* **4**, 1707 (2013).
- 39. Kaushik, A. *et al.* Magnetically guided central nervous system delivery and toxicity evaluation of magnetoelectric nanocarriers. *Sci. Rep.* **6**, 25309 (2016).
  - 40. Wang, P. *et al.* Colossal Magnetoelectric Effect in Core–Shell Magnetoelectric Nanoparticles. *Nano Lett.* **20**, 5765–5772 (2020).

- 41. Landau, L. D. & Haar, D. ter. *Collected Papers of L.D. Landau*. (Pergamon Press, Oxford London Edinburgh, 1965).
- 42. Mushtaq, F. *et al.* Magnetoelectrically Driven Catalytic Degradation of Organics. *Adv. Mater.* **31**, 1901378 (2019).
- 5 43. Fiocchi, S. *et al.* Modelling of magnetoelectric nanoparticles for non-invasive brain stimulation: a computational study. *J. Neural Eng.* **19**, 056020 (2022).

20

- 44. Jang, J. & Park, C. B. Magnetoelectric dissociation of Alzheimer's β-amyloid aggregates. *Sci. Adv.* **8**, eabn1675 (2022).
- 45. Raimondo, J. V., Burman, R. J., Katz, A. A. & Akerman, C. J. Ion dynamics during seizures. *Front. Cell. Neurosci.* 9, (2015).
- 46. Zhang, E. *et al.* Ab Initio Physics Considerations in the Design of Wireless and Non-Invasive Neural Recording Systems Using Magnetoelectric Nanoparticles. *IEEE Trans. Magn.* **59**, 1–5 (2023).
- 47. Corral-Flores, V., Bueno-Baqués, D. & Ziolo, R. F. Synthesis and characterization of novel CoFe2O4–BaTiO3 multiferroic core–shell-type nanostructures. *Acta Mater.* **58**, 764–769 (2010).
- 48. Marrella, A. *et al.* Magnetoelectric nanoparticles shape modulates their electrical output. *Front. Bioeng. Biotechnol.* **11**, 1219777 (2023).
  - 49. Chen, S. *et al.* Magnetic Properties of Magnetoelectric Nanoparticles With Varying Core–Shell Ratios and Their Effects on In Vitro Neuron Stimulation. *IEEE Trans. Magn.* **59**, 1–4 (2023).
  - 50. Kim, Y. J. *et al.* Magnetoelectric Nanodiscs Enable Wireless Transgene-Free Neuromodulation. Preprint at https://doi.org/10.1101/2023.12.24.573272 (2023).
  - 51. Pardo, M. & Khizroev, S. Where do we stand now regarding treatment of psychiatric and neurodegenerative disorders? Considerations in using magnetoelectric nanoparticles as an innovative approach. *WIREs Nanomedicine Nanobiotechnology* **14**, e1781 (2022).
  - 52. Smith, I. T. *et al.* Nanomedicine and nanobiotechnology applications of magnetoelectric nanoparticles. *WIREs Nanomedicine Nanobiotechnology* **15**, e1849 (2023).
  - 53. Tada, M., Takeuchi, A., Hashizume, M., Kitamura, K. & Kano, M. A highly sensitive fluorescent indicator dye for calcium imaging of neural activity *in vitro* and *in vivo*. *Eur. J. Neurosci.* **39**, 1720–1728 (2014).
  - 54. Kayyali, H. & Durand, D. Effects of applied currents on epileptiform bursts in vitro. *Exp. Neurol.* **113**, 249–254 (1991).

# Submitted Manuscript: Confidential Template revised November 2022

- 55. Nakagawa, M. & Durand, D. Suppression of spontaneous epileptiform activity with applied currents. *Brain Res.* **567**, 241–247 (1991).
- 56. Stoner, E. C. & Wohlfarth, E. P. A mechanism of magnetic hysteresis in heterogeneous alloys. *IEEE Trans. Magn.* 27, 3475–3518 (1991).
- 57. Chikazumi, S., Graham, C. D. & Chikazumi, S. *Physics of Ferromagnetism*. (Clarendon Press; Oxford University Press, Oxford: New York, 1997).

10

- 58. Kulbacka, J. et al. Cell Membrane Transport Mechanisms: Ion Channels and Electrical Properties of Cell Membranes. in Transport Across Natural and Modified Biological Membranes and its Implications in Physiology and Therapy (eds. Kulbacka, J. & Satkauskas, S.) vol. 227 39–58 (Springer International Publishing, Cham, 2017).
- 59. Malhotra, N. *et al.* Potential Toxicity of Iron Oxide Magnetic Nanoparticles: A Review. *Molecules* **25**, 3159 (2020).
- 60. Stimphil, E. *et al.* Physics considerations in targeted anticancer drug delivery by magnetoelectric nanoparticles. *Appl. Phys. Rev.* **4**, 021101 (2017).
- 15 61. Pu-Ling Lu & Charap, S. H. High density magnetic recording media design and identification: susceptibility to thermal decay. *IEEE Trans. Magn.* **31**, 2767–2769 (1995).
  - 62. Khizroev, S., Liu, Y., Mountfield, K., Kryder, M. H. & Litvinov, D. Physics of perpendicular magnetic recording: writing process. *J. Magn. Magn. Mater.* **246**, 335–344 (2002).
  - 63. Friedrich, J., Zhou, P. & Paninski, L. Fast online deconvolution of calcium imaging data. *PLOS Comput. Biol.*13, e1005423 (2017).
  - 64. Yu, Z. *et al.* Beyond t test and ANOVA: applications of mixed-effects models for more rigorous statistical analysis in neuroscience research. *Neuron* **110**, 21–35 (2022).
  - 65. Lazic, S. E., Clarke-Williams, C. J. & Munafò, M. R. What exactly is 'N' in cell culture and animal experiments? *PLOS Biol.* **16**, e2005282 (2018).
- 25 66. Yue, K. *et al.* Magneto-Electric Nano-Particles for Non-Invasive Brain Stimulation. *PLoS ONE* 7, e44040 (2012).

Acknowledgements: The authors acknowledge the invaluable help and advice throughout the entire study of our esteemed colleagues Dr. Brian Noga, Dr. Patrick Ganzer, Dr. Ibolya Edit Andras and Dr. Laura Bianchi of the University of Miami, Dr. Xiaoming Jin of Indiana University, Dr. Ian Smith and Dr. Gyorgy Lur of the University of California – Irvine (UCI). They also appreciate the technical assistance of their teammates Mostafa Abdel-Mottaleb, Victoria Andre, Craig Scully-Clemmons, Emily Zhu, and Jieyuan Tian.

Conflict of Interest: The concept of using MENPs for medical applications was for the first time proposed by SK and PL, with its neuromodulation hypothesis described in their 2012 paper <sup>66</sup>. In 2016, PL and SK have co-founded a biotech start-up, Cellular Nanomed, to develop a wireless brain-machine interface (BMI) based on magnetoelectric nanoparticles.

# Funding:

15

20

25

30

National Science Foundation (NSF) grant ECCS-211082 (SK, PL)

Defense Advanced Research Projects Agency (DARPA) and Naval Information Warfare Center, Pacific (NIWC Pacific) Contract N66001-19-C-4019 (SK, PL)

#### **Author contributions:**

Conceptualization: SK, PL, EZ

Methodology: EZ, SK

Synthesis: EZ, SC

Measurements: EZ, MS, AS, CC, DR

Analysis: EZ Supervision: SK Writing: SK, EZ

**Competing interests:** SK and PL co-founded a technology startup, Cellular Nanomed, to create MENPs-based biomedical applications.

**Data and materials availability:** All data, code, and materials used in the analysis will be made available after completing a materials transfer agreement (MTA).

# **Supplementary Materials**

35 Figs. S1 to S10

Movie S1

Submitted Manuscript: Confidential Template revised November 2022